Paper 72

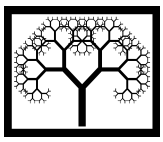

Proceedings of the Tenth International Conference
on Computational Structures Technology,
B.H.V. Topping, J.M. Adam, F.J. Pallarés,
R. Bru and M.L. Romero, (Editors),
Civil-Comp Press, Stirlingshire, Scotland

A Finite Deformation Exact Geometry Four-Node Solid-Shell Element for Piezoelectric Composite Structures

G.M. Kulikov and S.V. Plotnikova
Department of Applied Mathematics and Mechanics
Tambov State Technical University, Russia

Abstract

The present work focuses on the development of the finite rotation exact geometry (EG) piezoelectric four-node solid-shell element based on the first-order 7-parameter equivalent single-layer theory. The term EG reflects the fact that reference surface geometry is described by analytically given functions, that is, coefficients of the first and second fundamental forms are taken exactly at each element node. As fundamental shell unknowns, six tangential and transverse displacements of outer surfaces and the transverse displacement of the midsurface are chosen. Such choice of displacements gives the possibility to derive strain-displacement relationships, which are invariant under arbitrarily large rigid-body shell motions in a convected curvilinear coordinate system. It is assumed also that the electric potential is linear through the thickness of the piezoelectric layer and all seven displacements and electric potential degrees of freedom are coupled via constitutive equations. It is remarkable that elemental matrices require only direct substitutions and they are evaluated by using the 3D analytical integration.

Keywords: laminated piezoelectric shell, finite deformation, solid-shell element, 7-parameter model

1 Introduction

In recent years, a considerable progress has been achieved on the development of continuum-based finite elements that can handle geometrically linear [1-5] and nonlinear [6-9] analyses of thin piezoelectric laminated composite shells satisfactorily. These elements are typically defined by two layers of nodes at the bottom and top surfaces of the shell with three displacement degrees of freedom per node and known as isoparametric 6-parameter piezoelectric solid-shell elements. Unfortunately, a 6-parameter solid-shell element formulation based on the complete 3D constitutive equations is deficient because thickness locking occurs. This is due to the fact

that the linear displacement field in the thickness direction results in a constant transverse normal strain, which in turn causes artificial stiffening of the shell element in the case of non-vanishing Poisson's ratios. It should be mentioned that the errors caused by thickness locking do not decrease with the mesh refinement because the reason of stiffening lies in the shell theory itself rather than the finite element discretization. To prevent thickness locking, the 3D constitutive equations have to be modified employing generalized plane stress conditions [3, 4]. However, the use of complete 3D constitutive laws within the shell analysis is of great importance for engineering applications. In this aspect, the advanced finite element techniques were developed, namely, a hybrid stress method [1, 2] in which the transverse normal stress is constant through the thickness [10] and a most popular enhanced assumed strain method [5-9] in which the transverse normal strain is enriched in the thickness direction by a linear term [11].

To an alternative finite element formulation for the analysis of piezoelectric laminated structures one can arrive using EG solid-shell elements [12, 13]. The term EG is established in Abstract. The first EG piezoelectric solid-shell element is based on the 6-parameter equivalent single-layer (ESL) theory [12], which overcomes thickness locking by means of plane stress enforcement. The second one is based on the 7-parameter ESL theory [13], which permits to utilize complete 3D constitutive equations and is optimal with respect to a number of degrees of freedom employed [14-17]. Both EG piezoelectric solid-shell elements use geometrically linear strain-displacement relationships, which exactly represent small rigid-body shell motions in convected curvilinear coordinates [18]. In the present paper, the EG four-node solid-shell element formulation is extended to the analysis of piezoelectric laminated shell structures undergoing finite rotations. This finite element formulation is based on the geometrically non-linear 7-parameter ESL theory in which six tangential and transverse displacements of the outer surfaces and a transverse displacement of the midsurface are introduced as fundamental shell unknowns [19]. Such choice of displacements gives the possibility to represent the EG solid-shell element formulation developed in a very compact form and to derive non-linear strain-displacement relationships, which are invariant under arbitrarily large rigid-body shell motions in a convected curvilinear coordinate system [19-21].

It is assumed that the electric potential is linear through the thickness of the piezoelectric layer and all displacement and electric potential degrees of freedom are coupled via 3D constitutive equations. The first assumption means that the electric field is constant through the thickness of the piezoelectric layer, which is in bending dominated situations not correct [22]. Note also that the electric charge conservation law never can be satisfied precisely. The analytical developments for piezoelectric beams [23] and plates [24] showed that the quadratic variation of the electric potential in the thickness direction is sufficient to solve this problem. However, the quadratic approximation of the electric potential leads to including additional degrees of freedom in a finite element formulation and seems to be excessive for the actuator shell analysis.

To avoid shear and membrane locking and have no spurious zero energy modes, the assumed strain and stress resultant fields are invoked. This approach was developed for the finite rotation 6- and 7-parameter EG solid-shell element formulations

by Kulikov and Plotnikova [19, 25, 26]. Herein, this hybrid stress-strain formulation is generalized to the finite rotation EG piezoelectric four-node solid-shell element based on the first-order 7-parameter ESL shell theory. Taking into account that displacement vectors of outer and middle surfaces of the shell are resolved in the reference surface frame, the proposed EG piezoelectric solid-shell element formulation has computational advantages compared to conventional isoparametric solid-shell element formulations, since it reduces the computational cost of numerical integration in the evaluation of the stiffness matrix. This is due to the facts that, first, all element matrices require only direct substitutions, i.e., no numerical matrix inversion is needed. The latter is unusual for the isoparametric hybrid/mixed shell element formulations. Secondly, we use the efficient 3D analytical integration [26, 27] that permits to employ coarse meshes. Therefore, the EG four-node solid-shell element developed is promising because of the fact that electric signals generated by sensors are fed into microprocessors, which in turn must activate a system of piezoelectric actuators in real time.

2 Strain-Displacement Relationships

Consider a shell built up in the general case by the arbitrary superposition across the wall thickness of N thin layers of the uniform thickness $h_n = z_n - z_{n-1}$ including the ℓth piezoelectric layer (PZT) as shown in Figure 1. The nth layer may be defined as a 3D body of volume V_n bounded by two surfaces Ω_{n-1} and Ω_n, located at the distances $|z_{n-1}|$ and $|z_n|$ measured with respect to the reference surface Ω, and the edge boundary surface Σ_n. It is assumed that the bounding surfaces Ω_{n-1} and Ω_n are continuous, sufficiently smooth and without any singularities. Let the reference surface Ω be referred to the orthogonal curvilinear coordinates θ_1 and θ_2, which are referred to the lines of principal curvatures of its surface, whereas the coordinate θ_3 is oriented along the unit vector $\mathbf{e}_3$ normal to the reference surface; $\mathbf{e}_1$ and $\mathbf{e}_2$ are the unit vectors tangent to the lines of principal curvatures. Here and in the following developments, the index n identifies the belonging of any quantity to the nth layer and runs from 1 to N; the index of the piezoelectric layer $\ell = i_1, i_2, \ldots, i_L$, where L is the number of piezoelectric layers bonded to the outer surfaces of the host structure or embedded into its body; Greek indices α, β range from 1 to 2; indices i, j range from 1 to 3; the superscript A identifies the belonging of any quantity to the bottom and top surfaces Ω^- and Ω^+, and takes values $-$ and $+$.

The displacement field is approximated in the thickness direction according to [19]:

$$u_\alpha = N^- u_\alpha^- + N^+ u_\alpha^+, \qquad u_3 = L^- u_3^- + L^{\mathrm{M}} u_3^{\mathrm{M}} + L^+ u_3^+, \tag{1}$$

$$N^- = \frac{1}{h}\left(z^+ - \theta_3\right), \qquad N^+ = \frac{1}{h}\left(\theta_3 - z^-\right), \tag{2}$$

$$L^- = N^-\left(N^- - N^+\right), \qquad L^{\mathrm{M}} = 4N^- N^+, \qquad L^+ = N^+\left(N^+ - N^-\right), \tag{3}$$

where $N^A(\theta_3)$ and $L^A(\theta_3)$, $L^{\mathrm{M}}(\theta_3)$ are the Lagrange polynomials of the first and second orders, respectively; $h = z^+ - z^-$ is the thickness of the shell; $z^- = z_0$ and $z^+ = z_N$ are the transverse coordinates of bottom and top surfaces of the shell; $u_i^A(\theta_1, \theta_2)$ are the components of the displacement vectors of the bottom and top surfaces; $u_3^{\mathrm{M}}(\theta_1, \theta_2)$ is the transverse displacement of the midsurface Ω^{M} .

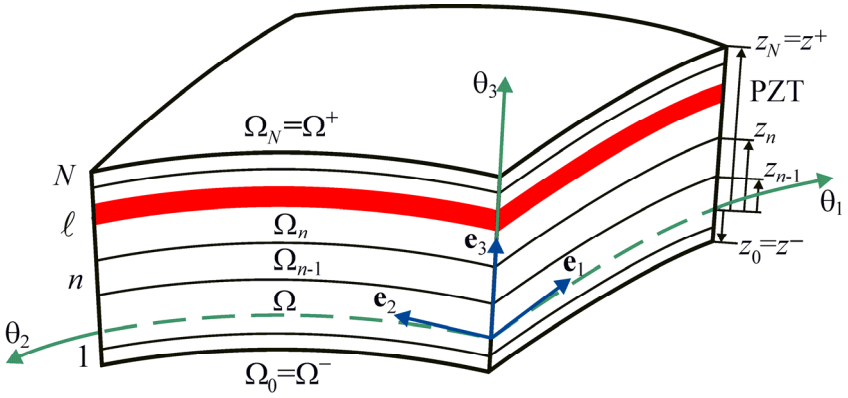

Figure 1: Laminated shell with embedded piezoelectric layer (PZT)

Next, we represent displacement vectors of outer surfaces in the reference surface frame as follows:

$$\mathbf{u}^A = \sum_i u_i^A \mathbf{e}_i. \tag{4}$$

Therefore, the strain-displacement relationships of the first-order 7-parameter shell model [19] can be written as

$$\varepsilon_{\alpha\beta} = N^- \varepsilon_{\alpha\beta}^- + N^+ \varepsilon_{\alpha\beta}^+, \qquad \varepsilon_{33} = N^- \varepsilon_{33}^- + N^+ \varepsilon_{33}^+, \tag{5}$$
$$\varepsilon_{\alpha 3} = \varepsilon_{\alpha 3}^{\mathrm{M}}, \qquad \varepsilon_{\alpha 3}^{\mathrm{M}} = \frac{1}{2}\left(\varepsilon_{\alpha 3}^- + \varepsilon_{\alpha 3}^+\right).$$

Here, $\varepsilon_{ij}^A(\theta_1, \theta_2)$ are the components of the Green-Lagrange strain tensor of outer surfaces given by

$$2\varepsilon_{\alpha\beta}^A = c_\alpha^A \lambda_{\alpha\beta}^A + c_\beta^A \lambda_{\beta\alpha}^A + \sum_i \lambda_{i\alpha}^A \lambda_{i\beta}^A, \qquad 2\varepsilon_{33}^A = 2\beta_3^A + \sum_i \beta_i^A \beta_i^A, \tag{6}$$
$$2\varepsilon_{\alpha 3}^A = c_\alpha^A \beta_\alpha^A + \lambda_{3\alpha}^A + \sum_i \beta_i^A \lambda_{i\alpha}^A,$$

where

$$\lambda_{\alpha\alpha}^A = \frac{1}{A_\alpha} u_{\alpha,\alpha}^A + B_\beta u_\beta^A + k_\alpha u_3^A \quad \text{for} \quad \beta \neq \alpha, \tag{7}$$
$$\lambda_{\beta\alpha}^A = \frac{1}{A_\alpha} u_{\beta,\alpha}^A - B_\beta u_\alpha^A \quad \text{for} \quad \beta \neq \alpha,$$

$$\lambda_{3\alpha}^{A}=\frac{1}{A_\alpha}u_{3,\alpha}^{A}-k_\alpha u_\alpha^{A},\qquad \beta_\alpha^{A}=\frac{1}{h}\left(u_\alpha^{+}-u_\alpha^{-}\right),$$

$$\beta_3^{-}=\frac{1}{h}\left(-3u_3^{-}+4u_3^{\mathrm{M}}-u_3^{+}\right),\qquad \beta_3^{+}=\frac{1}{h}\left(u_3^{-}-4u_3^{\mathrm{M}}+3u_3^{+}\right),$$

$$c_\alpha^{A}=1+k_\alpha z^{A},\qquad B_\alpha=\frac{1}{A_\alpha A_\beta}A_{\beta,\alpha}\quad\text{for }\beta\neq\alpha,$$

where A_α and k_α are the Lamé coefficients and principal curvatures of the reference surface; c_α^{A} are the components of the shifter tensor at outer surfaces of the shell; the abbreviation $(\,)_{,\alpha}$ implies the partial derivatives with respect to coordinates θ_α. It is noteworthy that strain-displacement relationships (5) and (6) exactly represent large rigid-body shell motions in a convected curvilinear coordinate system [19].

3 Description of Electric Field

The electric potential inside the ℓth piezoelectric layer is also assumed to be linear in the thickness direction

$$\varphi_\ell=N_\ell^{-}\varphi_\ell^{-}+N_\ell^{+}\varphi_\ell^{+},\tag{8}$$

$$N_\ell^{-}=\frac{1}{h_\ell}\left(z_\ell-\theta_3\right),\qquad N_\ell^{+}=\frac{1}{h_\ell}\left(\theta_3-z_{\ell-1}\right),\tag{9}$$

where $\varphi_\ell^{A}\left(\theta_1,\theta_2\right)$ are the values of the electric potential on the bottom and top surfaces of the ℓth layer; $h_\ell=z_\ell-z_{\ell-1}$ is the thickness of the piezoelectric layer.

The relation between the electric field $\mathbf{E}^{(\ell)}$ and the electric potential φ_ℓ is given by

$$\mathbf{E}^{(\ell)}=-\boldsymbol{\nabla}\varphi_\ell,\tag{10}$$

that is,

$$E_\alpha^{(\ell)}=N_\ell^{-}E_\alpha^{(\ell)-}+N_\ell^{+}E_\alpha^{(\ell)+},\qquad E_3^{(\ell)}=-\frac{1}{h_\ell}\left(\varphi_\ell^{+}-\varphi_\ell^{-}\right),\tag{11}$$

$$E_\alpha^{(\ell)-}=-\frac{1}{A_\alpha}\varphi_{\ell,\alpha}^{-},\qquad E_\alpha^{(\ell)+}=-\frac{1}{A_\alpha}\varphi_{\ell,\alpha}^{+},$$

where $E_\alpha^{(\ell)A}$ are the tangential components of the electric field of the ℓth layer. It is seen that the normal component of the electric field $E_3^{(\ell)}$ is constant through the thickness of the piezoelectric layer. A short discussion on that is presented in Introduction.

4 Constitutive Equations

The constitutive equations of linear piezoelectricity [28] for the monoclinic piezoelectric layer with reflectional symmetry in surfaces parallel to the reference surface can be expressed as

$$\boldsymbol{\varepsilon} = \mathbf{A}^{(\ell)}\boldsymbol{\sigma}^{(\ell)} + \left(\mathbf{d}^{(\ell)}\right)^{\mathrm{T}}\mathbf{E}^{(\ell)}, \tag{12}$$

$$\mathbf{D}^{(\ell)} = \mathbf{d}^{(\ell)}\boldsymbol{\sigma}^{(\ell)} + \boldsymbol{\varsigma}^{(\ell)}\mathbf{E}^{(\ell)}, \tag{13}$$

where $\boldsymbol{\varepsilon}$ is the strain vector; $\boldsymbol{\sigma}^{(\ell)}$ is the stress vector; $\mathbf{E}^{(\ell)}$ is the electric field vector; $\mathbf{D}^{(\ell)}$ is the electric displacement vector; $\mathbf{A}^{(\ell)}$ is the elastic compliance matrix; $\mathbf{d}^{(\ell)}$ is the piezoelectric matrix; $\boldsymbol{\varsigma}^{(\ell)}$ is the dielectric matrix defined by

$$\boldsymbol{\varepsilon} = \left[\varepsilon_{11}\ \varepsilon_{22}\ \varepsilon_{33}\ 2\varepsilon_{23}\ 2\varepsilon_{13}\ 2\varepsilon_{12}\right]^{\mathrm{T}}, \quad \boldsymbol{\sigma}^{(\ell)} = \left[\sigma_{11}^{(\ell)}\ \sigma_{22}^{(\ell)}\ \sigma_{33}^{(\ell)}\ \sigma_{23}^{(\ell)}\ \sigma_{13}^{(\ell)}\ \sigma_{12}^{(\ell)}\right]^{\mathrm{T}}, \tag{14}$$

$$\mathbf{E}^{(\ell)} = \left[E_1^{(\ell)}\ E_2^{(\ell)}\ E_3^{(\ell)}\right]^{\mathrm{T}}, \quad \mathbf{D}^{(\ell)} = \left[D_1^{(\ell)}\ D_2^{(\ell)}\ D_3^{(\ell)}\right]^{\mathrm{T}},$$

$$\mathbf{A}^{(\ell)} = \begin{bmatrix} A_{11}^{(\ell)} & A_{12}^{(\ell)} & A_{13}^{(\ell)} & 0 & 0 & A_{16}^{(\ell)} \\ & A_{22}^{(\ell)} & A_{23}^{(\ell)} & 0 & 0 & A_{26}^{(\ell)} \\ & & A_{33}^{(\ell)} & 0 & 0 & A_{36}^{(\ell)} \\ & & & A_{44}^{(\ell)} & A_{45}^{(\ell)} & 0 \\ & & & & A_{55}^{(\ell)} & 0 \\ \text{sym.} & & & & & A_{66}^{(\ell)} \end{bmatrix}, \tag{15}$$

$$\mathbf{d}^{(\ell)} = \begin{bmatrix} 0 & 0 & 0 & d_{14}^{(\ell)} & d_{15}^{(\ell)} & 0 \\ 0 & 0 & 0 & d_{24}^{(\ell)} & d_{25}^{(\ell)} & 0 \\ d_{31}^{(\ell)} & d_{32}^{(\ell)} & d_{33}^{(\ell)} & 0 & 0 & d_{36}^{(\ell)} \end{bmatrix}, \quad \boldsymbol{\varsigma}^{(\ell)} = \begin{bmatrix} \varsigma_{11}^{(\ell)} & \varsigma_{12}^{(\ell)} & 0 \\ & \varsigma_{22}^{(\ell)} & 0 \\ \text{sym.} & & \varsigma_{33}^{(\ell)} \end{bmatrix}.$$

Solving constitutive equations (12) for stresses and substituting stresses in constitutive equations (13), one obtains

$$\boldsymbol{\sigma}^{(\ell)} = \mathbf{C}^{(\ell)}\boldsymbol{\varepsilon} - \left(\mathbf{e}^{(\ell)}\right)^{\mathrm{T}}\mathbf{E}^{(\ell)}, \tag{16}$$

$$\mathbf{D}^{(\ell)} = \mathbf{e}^{(\ell)}\boldsymbol{\varepsilon} + \in^{(\ell)}\mathbf{E}^{(\ell)}, \tag{17}$$

where $\mathbf{C}^{(\ell)}$ is the material stiffness matrix; $\mathbf{e}^{(\ell)}$ and $\in^{(\ell)}$ are the piezoelectric and dielectric matrices expressed as

$$\mathbf{C}^{(\ell)} = \left(\mathbf{A}^{(\ell)}\right)^{-1}, \quad \mathbf{e}^{(\ell)} = \mathbf{d}^{(\ell)}\mathbf{C}^{(\ell)}, \quad \in^{(\ell)} = \boldsymbol{\varsigma}^{(\ell)} - \mathbf{d}^{(\ell)}\mathbf{C}^{(\ell)}\left(\mathbf{d}^{(\ell)}\right)^{\mathrm{T}}. \tag{18}$$

5 Hu-Washizu Variational Equation

A first-order 7-parameter piezoelectric ESL shell theory developed is based on the approximations of displacements (1), displacement-dependent strains (5), electric potential (8) and electric field (11) in the thickness direction. Additionally, we accept the through-thickness approximation for the independently assumed strains as follows:

$$\hat{\varepsilon}_{\alpha\beta} = N^{-}\hat{\varepsilon}^{-}_{\alpha\beta} + N^{+}\hat{\varepsilon}^{+}_{\alpha\beta}, \qquad \hat{\varepsilon}_{33} = N^{-}\hat{\varepsilon}^{-}_{33} + N^{+}\hat{\varepsilon}^{+}_{33}, \qquad \hat{\varepsilon}_{\alpha 3} = \hat{\varepsilon}^{\mathrm{M}}_{\alpha 3}, \tag{19}$$

where $\hat{\varepsilon}^{A}_{\alpha\beta}(\theta_1,\theta_2)$ and $\hat{\varepsilon}^{A}_{33}(\theta_1,\theta_2)$ are the assumed tangential and transverse normal strains of outer surfaces; $\hat{\varepsilon}^{\mathrm{M}}_{\alpha 3}(\theta_1,\theta_2)$ are the assumed transverse shear strains of the midsurface.

Substituting approximations (1), (5), (8), (11) and (19) into the 3D Hu-Washizu functional [12] and allowing for that metrics of all surfaces parallel to the reference surface are identical and equal to the metric of the midsurface, one arrives at the 2D Hu-Washizu functional for the 7-parameter shell element

$$\begin{aligned}\Pi^{\mathrm{el}}_{\mathrm{HW}} = \int_{-1}^{1}\int_{-1}^{1}\Big[&\frac{1}{2}\hat{\mathfrak{E}}^{\mathrm{T}}\mathbf{D}_{uu}\hat{\mathfrak{E}} - \hat{\mathfrak{E}}^{\mathrm{T}}\mathbf{D}^{(\ell)}_{u\varphi}\mathfrak{E}^{(\ell)} - \frac{1}{2}\big(\mathfrak{E}^{(\ell)}\big)^{\mathrm{T}}\mathbf{D}^{(\ell)}_{\varphi\varphi}\mathfrak{E}^{(\ell)} \\ &- \mathbf{H}^{\mathrm{T}}\big(\hat{\mathfrak{E}} - \mathfrak{E}\big) - \mathbf{v}^{\mathrm{T}}\mathbf{p} - \boldsymbol{\chi}^{\mathrm{T}}_{\ell}\mathbf{q}_{\ell}\Big]\, A_1A_2c^{\mathrm{M}}_1c^{\mathrm{M}}_2\ell_1\ell_2\mathrm{d}\xi_1\mathrm{d}\xi_2.\end{aligned} \tag{20}$$

Here, more convenient matrix notations are introduced

$$\begin{aligned}\mathbf{v} &= \big[u^{-}_1\ u^{-}_2\ u^{-}_3\ u^{+}_1\ u^{+}_2\ u^{+}_3\ u^{\mathrm{M}}_3\big]^{\mathrm{T}}, \quad \boldsymbol{\chi}_{\ell} = \big[\varphi^{-}_{\ell}\ \varphi^{+}_{\ell}\big]^{\mathrm{T}}, \\ \mathfrak{E} &= \big[\varepsilon^{-}_{11}\ \varepsilon^{+}_{11}\ \varepsilon^{-}_{22}\ \varepsilon^{+}_{22}\ \varepsilon^{-}_{33}\ \varepsilon^{+}_{33}\ 2\varepsilon^{-}_{12}\ 2\varepsilon^{+}_{12}\ 2\varepsilon^{\mathrm{M}}_{13}\ 2\varepsilon^{\mathrm{M}}_{23}\big]^{\mathrm{T}}, \\ \hat{\mathfrak{E}} &= \big[\hat{\varepsilon}^{-}_{11}\ \hat{\varepsilon}^{+}_{11}\ \hat{\varepsilon}^{-}_{22}\ \hat{\varepsilon}^{+}_{22}\ \hat{\varepsilon}^{-}_{33}\ \hat{\varepsilon}^{+}_{33}\ 2\hat{\varepsilon}^{-}_{12}\ 2\hat{\varepsilon}^{+}_{12}\ 2\hat{\varepsilon}^{\mathrm{M}}_{13}\ 2\hat{\varepsilon}^{\mathrm{M}}_{23}\big]^{\mathrm{T}}, \\ \mathbf{H} &= \big[H^{-}_{11}\ H^{+}_{11}\ H^{-}_{22}\ H^{+}_{22}\ H^{-}_{33}\ H^{+}_{33}\ H^{-}_{12}\ H^{+}_{12}\ H_{13}\ H_{23}\big]^{\mathrm{T}}, \\ \mathfrak{E}^{(\ell)} &= \big[E^{(\ell)-}_1\ E^{(\ell)+}_1\ E^{(\ell)-}_2\ E^{(\ell)+}_2\ E^{(\ell)}_3\big]^{\mathrm{T}}, \\ \mathbf{p} &= \big[-p^{-}_1\ -p^{-}_2\ -p^{-}_3\ p^{+}_1\ p^{+}_2\ p^{+}_3\ 0\big]^{\mathrm{T}}, \quad \mathbf{q}_{\ell} = \big[q^{-}_{\ell}\ q^{+}_{\ell}\big]^{\mathrm{T}},\end{aligned} \tag{21}$$

where $\mathbf{D}_{uu}$, $\mathbf{D}^{(\ell)}_{u\varphi}$ and $\mathbf{D}^{(\ell)}_{\varphi\varphi}$ are the mechanical, piezoelectric and dielectric constitutive matrices presented in Appendix A; $\xi_{\alpha} = (\theta_{\alpha} - d_{\alpha})/\ell_{\alpha}$ are the normalized curvilinear elemental coordinates shown in Figure 2; d_{α} are the coordinates of the center of the element; $2\ell_{\alpha}$ are the lengths of the element in θ_{α}-directions; $c^{\mathrm{M}}_{\alpha} = 1 + k_{\alpha}z^{\mathrm{M}}$ are the components of the shifter tensor at the midsurface; $z^{\mathrm{M}} = \big(z^{-} + z^{+}\big)/2$ is the transverse coordinate of the midsurface; p^{A}_{i} are the tractions applied to the bottom and top surfaces; q^{A}_{ℓ} are the prescribed surface charge densities of the ℓth piezoelectric layer; $H^{\pm}_{\alpha\beta}$, $H^{\pm}_{33}$ and $H_{\alpha 3}$ are the stress resultants defined as

$$H^{A}_{\alpha\beta} = \sum_{n}\int_{z_{n-1}}^{z_n}\sigma^{(n)}_{\alpha\beta}N^{A}\mathrm{d}\theta_3, \qquad H^{A}_{33} = \sum_{n}\int_{z_{n-1}}^{z_n}\sigma^{(n)}_{33}N^{A}\mathrm{d}\theta_3, \qquad H_{\alpha 3} = \sum_{n}\int_{z_{n-1}}^{z_n}\sigma^{(n)}_{\alpha 3}\mathrm{d}\theta_3. \tag{22}$$

Remark 1. For the simplicity, we limit our discussion to the case of one piezoelectric layer, i.e., $L = 1$ and $\ell = i_1 \in \{1, 2, \ldots, N\}$, since only a sign of the summation needs to be involved in Equation (20) to generalize.

Using the stationarity of the Hu-Washizu functional (20) with respect to indepen-

dent variables $\mathbf{v}$, $\hat{\boldsymbol{\varepsilon}}$, $\mathbf{H}$ and $\boldsymbol{\chi}_\ell$, one can write the mixed variational equation as follows:

$$\delta \Pi^{\mathrm{el}}_{\mathrm{HW}} = 0. \tag{23}$$

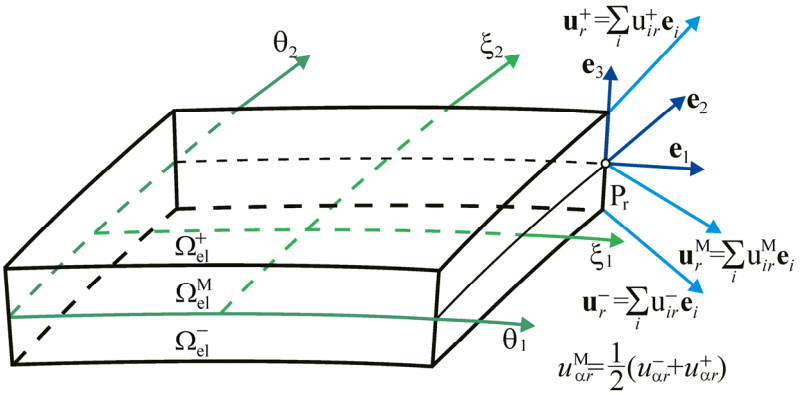

Figure 2: EG piezoelectric solid-shell element based on the 7-parameter ESL shell model, where P_r is the element node ($r = 1,2,\ldots,NN$)

6 Finite Element Formulation

The finite element formulation is based on the simple and efficient approximation of shells via *curved four-node* piezoelectric solid-shell elements

$$\mathbf{v} = \sum_r N_r \mathbf{v}_r, \qquad \mathbf{v}_r = \left[u^-_{1r}\ u^-_{2r}\ u^-_{3r}\ u^+_{1r}\ u^+_{2r}\ u^+_{3r}\ u^{\mathrm{M}}_{3r}\right]^{\mathrm{T}}, \tag{24}$$

$$\boldsymbol{\chi}_\ell = \sum_r N_r \boldsymbol{\chi}_{\ell r}, \qquad \boldsymbol{\chi}_{\ell r} = \left[\varphi^-_{\ell r}\ \varphi^+_{\ell r}\right]^{\mathrm{T}}, \tag{25}$$

where $N_r(\xi_1,\xi_2)$ are the bilinear shape functions of the element; $\mathbf{v}_r$ and $\boldsymbol{\chi}_{\ell r}$ are the displacement and electric potential vectors of the element nodes; the index r runs from 1 to 4 and denotes the number of nodes.

To implement the analytical integration throughout the element, we employ the *assumed interpolations* of natural strains and electric potentials [12, 13]

$$\mathfrak{E} = \sum_r N_r \mathfrak{E}_r, \qquad \mathfrak{E}_r = \mathfrak{E}(\mathrm{P}_r), \tag{26}$$

$$\mathfrak{E}^{(\ell)} = \sum_r N_r \mathfrak{E}^{(\ell)}_r, \qquad \mathfrak{E}^{(\ell)}_r = \mathfrak{E}^{(\ell)}(\mathrm{P}_r). \tag{27}$$

Introducing the displacement and electric potential vectors of the shell element

$$\mathbf{U} = \left[\mathbf{v}_1^{\mathrm{T}}\ \mathbf{v}_2^{\mathrm{T}}\ \mathbf{v}_3^{\mathrm{T}}\ \mathbf{v}_4^{\mathrm{T}}\right]^{\mathrm{T}}, \tag{28}$$

$$\mathbf{\Phi}_\ell = \left[\boldsymbol{\chi}_{\ell 1}^{\mathrm{T}}\ \boldsymbol{\chi}_{\ell 2}^{\mathrm{T}}\ \boldsymbol{\chi}_{\ell 3}^{\mathrm{T}}\ \boldsymbol{\chi}_{\ell 4}^{\mathrm{T}}\right]^{\mathrm{T}}, \tag{29}$$

one derives the following presentations of nodal strain and electric field vectors:

$$\mathfrak{E}_r = \mathbf{B}_r^u\mathbf{U} + \left(\mathbf{A}_r^u\mathbf{U}\right)\mathbf{U} = \left(\mathbf{B}_r^u + \mathbf{A}_r^u\mathbf{U}\right)\mathbf{U}, \tag{30}$$

$$\mathfrak{E}_r^{(\ell)} = -\mathbf{B}_r^{\varphi(\ell)}\mathbf{\Phi}_\ell, \tag{31}$$

where $\mathbf{B}_r^u$ are the nodal matrices of order 10×28 corresponding to the linear strain-displacement transformation (6); $\mathbf{A}_r^u$ are the nodal 3D arrays of order $10\times 28\times 28$ corresponding to the non-linear strain-displacement transformation (6); $\mathbf{B}_r^{\varphi(\ell)}$ are the nodal matrices of order 5×8 corresponding to the electric field transformation (11). The explicit presentations of nodal matrices $\mathbf{B}_r^u$ and $\mathbf{B}_r^{\varphi(\ell)}$ can be found in [13].

From the computational point of view it is convenient to rewrite interpolations (26) and (27) as follows:

$$\mathfrak{E} = \sum_{r_1,r_2}\left(\xi_1\right)^{r_1}\left(\xi_2\right)^{r_2}\mathfrak{E}^{r_1r_2}, \qquad \mathfrak{E}^{r_1r_2} = \left(\mathbf{B}_u^{r_1r_2} + \mathbf{A}_u^{r_1r_2}\mathbf{U}\right)\mathbf{U}, \tag{32}$$

$$\mathfrak{E}^{(\ell)} = \sum_{r_1,r_2}\left(\xi_1\right)^{r_1}\left(\xi_2\right)^{r_2}\mathfrak{E}^{(\ell)r_1r_2}, \qquad \mathfrak{E}^{(\ell)r_1r_2} = -\mathbf{B}_\varphi^{(\ell)r_1r_2}\mathbf{\Phi}_\ell, \tag{33}$$

where the superscripts r_1, r_2 take the values 0 and 1, and

$$\mathbf{B}_u^{00} = \frac{1}{4}\left(\mathbf{B}_1^u + \mathbf{B}_2^u + \mathbf{B}_3^u + \mathbf{B}_4^u\right), \qquad \mathbf{B}_u^{01} = \frac{1}{4}\left(\mathbf{B}_1^u + \mathbf{B}_2^u - \mathbf{B}_3^u - \mathbf{B}_4^u\right), \tag{34}$$

$$\mathbf{B}_u^{10} = \frac{1}{4}\left(\mathbf{B}_1^u - \mathbf{B}_2^u - \mathbf{B}_3^u + \mathbf{B}_4^u\right), \qquad \mathbf{B}_u^{11} = \frac{1}{4}\left(\mathbf{B}_1^u - \mathbf{B}_2^u + \mathbf{B}_3^u - \mathbf{B}_4^u\right).$$

The matrices $\mathbf{B}_\varphi^{(\ell)r_1r_2}$ and 3D arrays $\mathbf{A}_u^{r_1r_2}$ are written in a similar manner.

To avoid shear and membrane locking and have no spurious zero energy modes, the assumed displacement-independent strain and stress resultant fields throughout the element are invoked

$$\hat{\mathfrak{E}} = \sum_{r_1,r_2}\left(\xi_1\right)^{r_1}\left(\xi_2\right)^{r_2}\mathbf{Q}^{r_1r_2}\hat{\mathfrak{E}}^{r_1r_2}, \tag{35}$$

$$\hat{\mathfrak{E}}^{00} = \left[\hat{\varepsilon}_{11}^{-00}\ \hat{\varepsilon}_{11}^{+00}\ \hat{\varepsilon}_{22}^{-00}\ \hat{\varepsilon}_{22}^{+00}\ \hat{\varepsilon}_{33}^{-00}\ \hat{\varepsilon}_{33}^{+00}\ 2\hat{\varepsilon}_{12}^{-00}\ 2\hat{\varepsilon}_{12}^{+00}\ 2\hat{\varepsilon}_{13}^{\mathrm{M}00}\ 2\hat{\varepsilon}_{23}^{\mathrm{M}00}\right]^{\mathrm{T}},$$

$$\hat{\mathfrak{E}}^{01} = \left[\hat{\varepsilon}_{11}^{-01}\ \hat{\varepsilon}_{11}^{+01}\ \hat{\varepsilon}_{33}^{-01}\ \hat{\varepsilon}_{33}^{+01}\ 2\hat{\varepsilon}_{13}^{\mathrm{M}01}\right]^{\mathrm{T}}, \qquad \hat{\mathfrak{E}}^{10} = \left[\hat{\varepsilon}_{22}^{-10}\ \hat{\varepsilon}_{22}^{+10}\ \hat{\varepsilon}_{33}^{-10}\ \hat{\varepsilon}_{33}^{+10}\ 2\hat{\varepsilon}_{23}^{\mathrm{M}10}\right]^{\mathrm{T}},$$

$$\hat{\mathfrak{E}}^{11} = \left[\hat{\varepsilon}_{33}^{-11}\ \hat{\varepsilon}_{33}^{+11}\right]^{\mathrm{T}},$$

$$\mathbf{H} = \sum_{r_1,r_2}\left(\xi_1\right)^{r_1}\left(\xi_2\right)^{r_2}\mathbf{Q}^{r_1r_2}\mathbf{H}^{r_1r_2}, \tag{36}$$

$$\mathbf{H}^{00} = \left[H_{11}^{-00}\ H_{11}^{+00}\ H_{22}^{-00}\ H_{22}^{+00}\ H_{33}^{-00}\ H_{33}^{+00}\ H_{12}^{-00}\ H_{12}^{+00}\ H_{13}^{00}\ H_{23}^{00}\right]^{\mathrm{T}},$$

$$\mathbf{H}^{01} = \left[H_{11}^{-01}H_{11}^{+01}H_{33}^{-01}H_{33}^{+01}H_{13}^{01}\right]^{\mathrm{T}}, \qquad \mathbf{H}^{10} = \left[H_{22}^{-10}H_{22}^{+10}H_{33}^{-10}H_{33}^{+10}H_{23}^{10}\right]^{\mathrm{T}},$$

$$\mathbf{H}^{11} = \left[H_{33}^{-11}\ H_{33}^{+11}\right]^{\mathrm{T}},$$

$$\mathbf{Q}^{01}=\begin{bmatrix}1&0&0&0&0\\0&1&0&0&0\\0&0&0&0&0\\0&0&0&0&0\\0&0&1&0&0\\0&0&0&1&0\\0&0&0&0&0\\0&0&0&0&0\\0&0&0&0&1\\0&0&0&0&0\end{bmatrix},\quad \mathbf{Q}^{10}=\begin{bmatrix}0&0&0&0&0\\0&0&0&0&0\\1&0&0&0&0\\0&1&0&0&0\\0&0&1&0&0\\0&0&0&1&0\\0&0&0&0&0\\0&0&0&0&0\\0&0&0&0&0\\0&0&0&0&1\end{bmatrix},\quad \mathbf{Q}^{11}=\begin{bmatrix}0&0\\0&0\\0&0\\0&0\\1&0\\0&1\\0&0\\0&0\\0&0\\0&0\end{bmatrix}, \tag{37}$$

where $\mathbf{Q}^{00}$ is the identity matrix of order 10×10.

Substituting interpolations (24), (25), (32), (33), (35) and (36) into the mixed variational equation (23) in conjunction with (20) and using the *analytical integration* inside the element, one obtains the element equilibrium equations

$$\hat{\boldsymbol{\mathfrak{E}}}^{r_1r_2}=\left(\mathbf{Q}^{r_1r_2}\right)^{\mathrm{T}}\left(\mathbf{B}_u^{r_1r_2}+\mathbf{A}_u^{r_1r_2}\mathbf{U}\right)\mathbf{U}, \tag{38}$$

$$\mathbf{H}^{r_1r_2}=\left(\mathbf{Q}^{r_1r_2}\right)^{\mathrm{T}}\mathbf{D}_{uu}\mathbf{Q}^{r_1r_2}\hat{\boldsymbol{\mathfrak{E}}}^{r_1r_2}+\left(\mathbf{Q}^{r_1r_2}\right)^{\mathrm{T}}\mathbf{D}_{u\varphi}^{(\ell)}\mathbf{B}_{\varphi}^{(\ell)r_1r_2}\boldsymbol{\Phi}_{\ell}, \tag{39}$$

$$\sum_{r_1,r_2}\frac{1}{3^{r_1+r_2}}\left(\mathbf{B}_u^{r_1r_2}+2\mathbf{A}_u^{r_1r_2}\mathbf{U}\right)^{\mathrm{T}}\mathbf{Q}^{r_1r_2}\mathbf{H}^{r_1r_2}=\mathbf{F}_{\mathrm{p}}, \tag{40}$$

$$\sum_{r_1,r_2}\frac{1}{3^{r_1+r_2}}\left(\mathbf{B}_{\varphi}^{(\ell)r_1r_2}\right)^{\mathrm{T}}\left[\left(\mathbf{D}_{u\varphi}^{(\ell)}\right)^{\mathrm{T}}\mathbf{Q}^{r_1r_2}\hat{\boldsymbol{\mathfrak{E}}}^{r_1r_2}-\mathbf{D}_{\varphi\varphi}^{(\ell)}\mathbf{B}_{\varphi}^{(\ell)r_1r_2}\boldsymbol{\Phi}_{\ell}\right]=\mathbf{F}_{\mathrm{q}}^{(\ell)}, \tag{41}$$

where $\mathbf{F}_{\mathrm{p}}$ is the element-wise surface traction vector; $\mathbf{F}_{\mathrm{q}}^{(\ell)}$ is the element-wise electric force vector of the ℓth piezoelectric layer.

For the actuator-embedded shell analysis when only a prescribed input voltage is applied, the non-linear finite element equations are simplified because Eq. (43) can be omitted. Employing further the Newton-Raphson iteration process

$$\mathbf{U}^{[k+1]}=\mathbf{U}^{[k]}+\Delta\mathbf{U}^{[k]},\qquad \hat{\boldsymbol{\mathfrak{E}}}^{r_1r_2[k+1]}=\hat{\boldsymbol{\mathfrak{E}}}^{r_1r_2[k]}+\Delta\hat{\boldsymbol{\mathfrak{E}}}^{r_1r_2[k]},\qquad \mathbf{H}^{r_1r_2[k+1]}=\mathbf{H}^{r_1r_2[k]}+\Delta\mathbf{H}^{r_1r_2[k]}\quad (k=0,1,\ldots), \tag{42}$$

eliminating assumed strains $\Delta\hat{\boldsymbol{\mathfrak{E}}}^{r_1r_2[k]}$ and stress resultants $\mathbf{H}^{r_1r_2[k]}$ from linearized equilibrium equations derived, we arrive at the governing finite element equations

$$\mathbf{K}_{\mathrm{T}}\Delta\mathbf{U}^{[k]}=\Delta\mathbf{F}^{[k]}, \tag{43}$$

where $\mathbf{K}_{\mathrm{T}}=\mathbf{K}_{\mathrm{D}}+\mathbf{K}_{\mathrm{H}}$ is the tangent stiffness matrix; $\Delta\mathbf{F}^{[k]}$ is the right hand side vector given by

$$\mathbf{K}_{\mathrm{D}}=\sum_{r_1,r_2}\frac{1}{3^{r_1+r_2}}\left(\mathbf{L}^{r_1r_2[k]}\right)^{\mathrm{T}}\mathbf{D}^{r_1r_2}\mathbf{L}^{r_1r_2[k]}, \tag{44}$$

$$\mathbf{K}_{\mathrm{H}}=2\sum_{r_1,r_2}\frac{1}{3^{r_1+r_2}}\left(\mathbf{Q}^{r_1r_2}\mathbf{H}^{r_1r_2[k]}\right)\mathbf{A}_u^{r_1r_2},$$

$$\Delta\mathbf{F}^{[k]} = \mathbf{F}_p - \sum_{r_1,r_2} \frac{1}{3^{r_1+r_2}} \left(\mathbf{L}^{r_1 r_2}[k]\right)^{\mathrm{T}} \left[\mathbf{D}^{r_1 r_2}\left(\mathbf{L}^{r_1 r_2}[k] - \mathbf{A}_u^{r_1 r_2}\mathbf{U}^{[k]}\right)\mathbf{U}^{[k]} + \mathbf{Q}^{r_1 r_2}\boldsymbol{\Pi}_\ell^{r_1 r_2}\right],$$

where

$$\mathbf{L}^{r_1 r_2}[k] = \mathbf{B}_u^{r_1 r_2} + 2\mathbf{A}_u^{r_1 r_2}\mathbf{U}^{[k]}, \qquad \boldsymbol{\Pi}_\ell^{r_1 r_2} = \left(\mathbf{Q}^{r_1 r_2}\right)^{\mathrm{T}} \mathbf{D}_{u\varphi}^{(\ell)} \mathbf{B}_\varphi^{(\ell) r_1 r_2} \boldsymbol{\Phi}_\ell, \tag{45}$$

$$\mathbf{D}^{r_1 r_2} = \mathbf{Q}^{r_1 r_2}\overline{\mathbf{D}}^{r_1 r_2}\left(\mathbf{Q}^{r_1 r_2}\right)^{\mathrm{T}}, \qquad \overline{\mathbf{D}}^{r_1 r_2} = \left(\mathbf{Q}^{r_1 r_2}\right)^{\mathrm{T}} \mathbf{D}_{uu} \mathbf{Q}^{r_1 r_2}.$$

Remark 2. The tangent stiffness matrix $\mathbf{K}_{\mathrm{T}}$ is symmetric. This is due to the fact that both matrices $\mathbf{K}_{\mathrm{D}}$ and $\mathbf{K}_{\mathrm{H}}$ are symmetric. The proof of symmetry of the latter matrix can be found in [19].

Remark 3. The element stiffness matrix possesses a correct rank because 22 assumed strain parameters are adopted according to interpolation (35). It is necessary to note that the elemental matrices (44), (45) require only direct substitutions, i.e., no expensive matrix inversion is needed to derive them. This is unusual for the isoparametric hybrid/mixed finite element formulations. Furthermore, all matrices are evaluated by using analytical integration throughout the element.

The equilibrium equations (43) for each element are assembled by the usual technique to form the global equilibrium equations. These equations have to be performed until the required accuracy of the solution can be obtained. Herein, two convergence criteria are employed to describe more carefully high potential of the proposed finite element formulation, namely,

$$\left\| \mathbf{U}_G^{[k+1]} - \mathbf{U}_G^{[k]} \right\| < \varepsilon \left\| \mathbf{U}_G^{[k]} \right\| \tag{46}$$

and

$$\left\| \mathbf{r}^{[k]} \right\| < \varepsilon \left\| \mathbf{r}^{[0]} \right\|, \tag{47}$$

where $\|\bullet\|$ stands for the Euclidean norm; $\mathbf{U}_G$ is the global displacement vector; $\mathbf{r}$ is the residual vector; ε is the prescribed tolerance.

7 Numerical Examples

The performance of the proposed non-linear piezoelectric four-node solid-shell element EG7P4 is evaluated with several discriminating problems extracted from the literature and authors' example as well. For this purpose the following notations are introduced: NI is the number of the Newton iteration; RN is the Euclidean norm of the residual vector $\mathbf{r}^{[\mathrm{NI}]}$; DN is the Euclidean norm of the difference of global displacement vectors $\mathbf{U}_G^{[\mathrm{NI}+1]} - \mathbf{U}_G^{[\mathrm{NI}]}$. Note also that computations were performed on a standard PC Pentium using Delphi environment.

7.1 Geometrically Linear Examples

7.1.1 Cantilever Plate with Segmented Actuators

Consider a cantilever laminated plate with segmented PZT G1195 actuators attached to its bottom and top surfaces [29] as shown in Figure 3. The plate core is composed of six AS4/3501 graphite/epoxy layers with stacking sequences $[30/30/0]_s$ and $[0/45/\text{-}45]_s$. The geometrical data of the problem are taken as $a = 292$ mm, $b = 152$ mm, $h_C = 0.83$ mm and $h_{PZT} = 0.25$ mm. The elastic and piezoelectric material properties are shown in Table 1.

Property	Piezoceramic G1195	Graphite/ Epoxy AS4/3501	Composite (Section 7.2.2)	Piezoceramic (Section 7.2.2)
E_1 (GPa)	63	143	400	20
E_2, E_3 (GPa)	63	9.7	10	20
ν_{12}, ν_{13}	0.3	0.3	0.25	0.3
ν_{23}	0.3	0.3	0.25	0.3
G_{12}, G_{13} (GPa)	24.2	6	6	7.7
G_{23} (GPa)	24.2	2	6	7.7
d_{31}, d_{32} (nm/V)	0.254	0	0	2
d_{33} (nm/V)	0.374	0	0	0

Table 1: Elastic and piezoelectric material properties

The piezoceramic layers are polarized in opposite directions parallel to the thickness direction and subjected to opposite electric potentials $-\hat{\varphi}$ and $\hat{\varphi}$ to the outer patches surfaces to induce the bending actuation. The electrodes on the interfaces are assumed to be at the zero potential. A plate is modeled by the non-uniform 16×10 mesh of EG7P4 elements depicted in Figure 3.

Figures 4-6 display the distribution of dimensionless midplane displacements $w_1 = u_3^{\mathrm{M}}(\mathrm{B})/b$ and $w_2 = \left(u_3^{\mathrm{M}}(\mathrm{C}) - u_3^{\mathrm{M}}(\mathrm{A})\right)/b$ along the x-axis. A comparison with the isoparametric four-node solid-shell element formulation [6] and experimental study [29] is also given. The results are presented for plates loaded statically at outer actuator surfaces by electric potentials of 188.8 V and 157.6 V. It is seen that both four-node solid-shell elements perform excellently.

7.1.2 Spiral Actuator

Consider a spiral actuator [30] made of the PZT-5H ceramic with the following properties: $c_{11} = c_{22} = 127.205$ GPa, $c_{12} = 80.212$ GPa, $c_{13} = c_{23} = 84.670$ GPa, $c_{33} = 117.436$ GPa, $c_{44} = c_{55} = 22.988$ GPa, $c_{66} = 23.474$ GPa, $e_{31} = e_{32} = -6.62$ C/m^2, $e_{33} = 23.24$ C/m^2, $e_{24} = e_{15} = 17.03$ C/m^2. The spiral, shown in Figure

6, consists of four turns and has external radii $r_{\min} = 1.875$ mm and $r_{\max} = 15.2$ mm, an effective length $L = 215$ mm, and a width $b = 3.75$ mm. The geometrical parameters of the spiral shell can be represented as

$$A_1 = 1, \quad A_2 = \sqrt{a^2 + r^2}, \quad k_1 = 0, \quad k_2 = \frac{1}{A_2^3}\left(2a^2 + r^2\right), \tag{48}$$

$$r = r_{\min} + a\theta_2, \quad \theta_2 \in [0, 8\pi],$$

where r is the polar radius; a is the parameter, which controls the distance between successive turnings. The actuator is polarized in the thickness direction and subjected to a constant voltage $\Delta V = 100$ V.

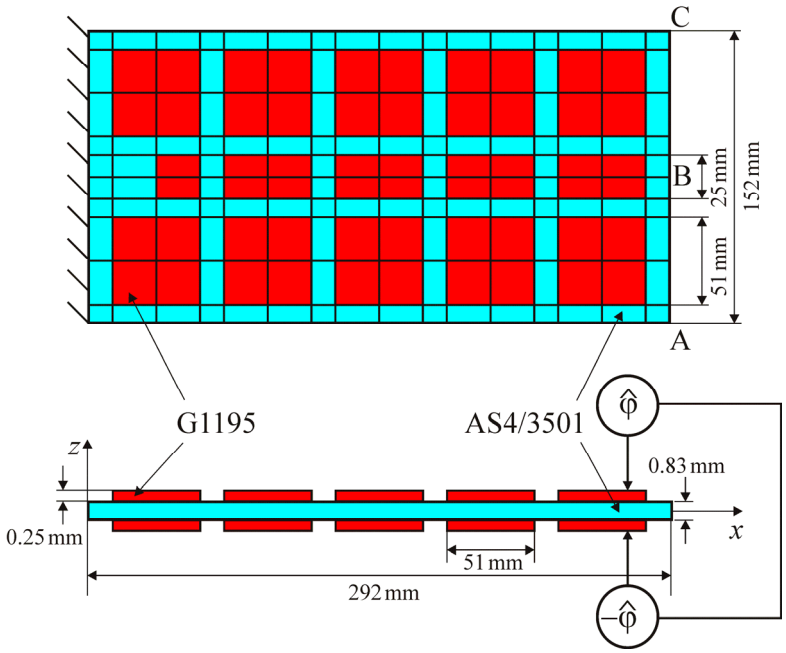

Figure 3: Cantilever plate with segmented actuators: geometry and mesh configuration

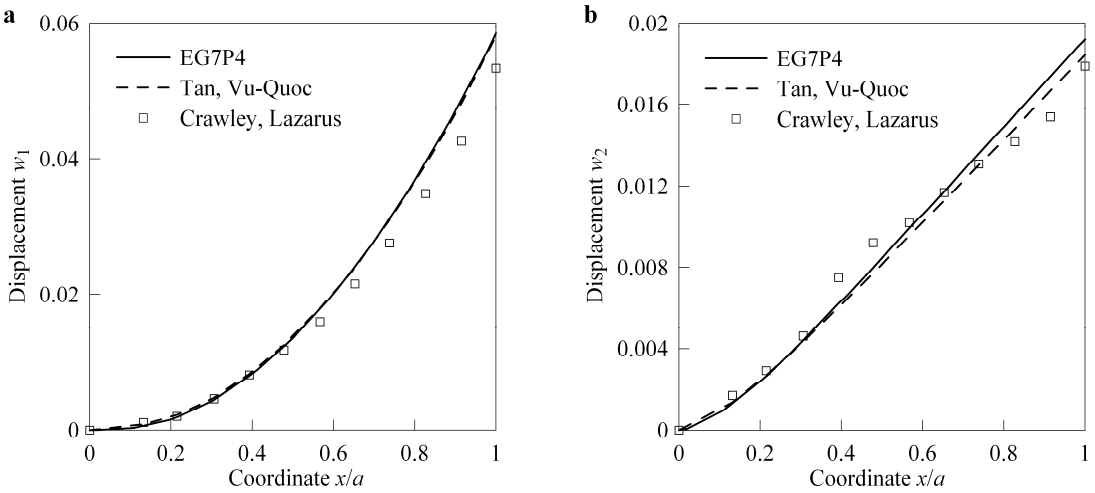

Figure 4: Dimensionless displacements of the $[30/30/0]_s$ plate in bending actuation subjected to a constant voltage $\hat{\varphi} = 188.8$ V : (a) w_1 and (b) w_2

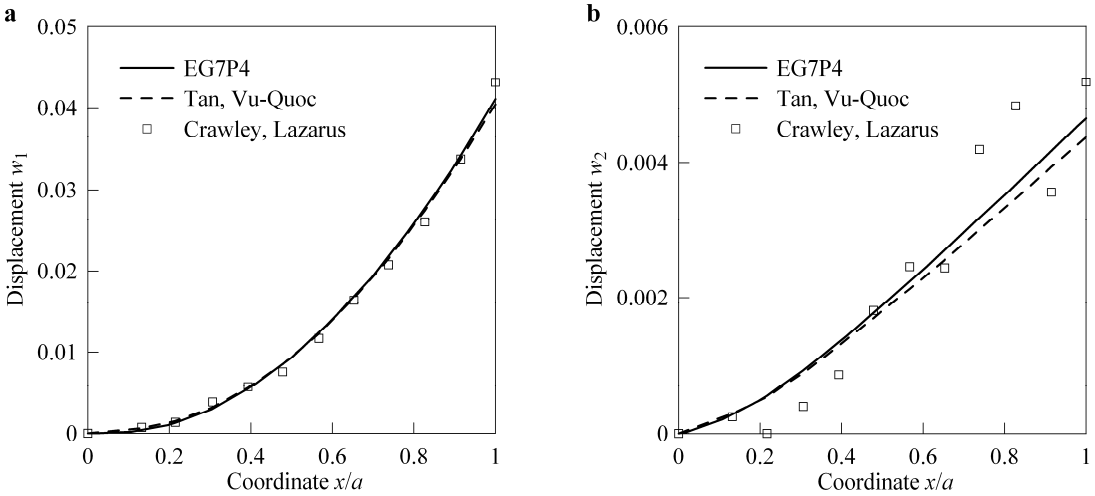

Figure 5: Dimensionless displacements of the $[0/45/-45]_s$ plate in bending actuation subjected to a constant voltage $\hat{\varphi} = 157.6\,\mathrm{V}$: (a) w_1 and (b) w_2

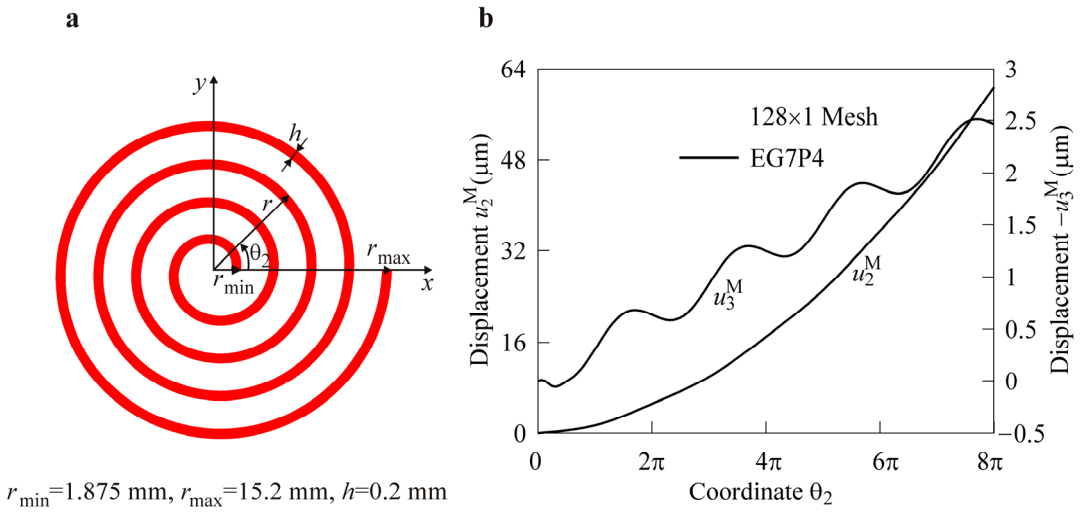

Figure 6: Spiral actuator: (a) geometry and (b) midsurface displacements

Element	EG7P4								Q_4TSF	C3D8E
Mesh	16×1	16×2	16×4	32×1	32×2	32×4	64×1	128×1	[30]	[30]
$-u_3^M\,(\mu\mathrm{m})$	2.109	2.102	2.100	2.625	2.620	2.619	2.503	2.460	2.00	2.59
$u_2^M\,(\mu\mathrm{m})$	58.18	58.16	58.15	59.95	59.88	59.87	60.55	60.72	-0.62	41.47

Table 2: Convergence results through using the tip midsurface displacements of the spiral actuator

A spiral shell is modeled by uniform meshes of EG7P4 elements. Table 2 lists the results of the convergence study due to mesh refinement considering the tangential and transverse midsurface displacements at the tip and a comparison with finite ele-

ment solutions [30]. The reference solution has been provided by the Abaqus® solid element C3D8E with a fine mesh, that is, two elements across the thickness and 20 elements across the width but the number of elements across the length is not documented. As can be seen, the EG7P4 element allows us to utilize coarse meshes because the 16×1 mesh yields already a good answer for the tangential displacement. Note also that the 7-parameter shell model overestimates the tangential tip displacement by 40 %. This can be explained by the fact that the layer-wise description should be employed. A comparison with the degenerated shell element Q_4TSF shows additionally that the d_{33}-effect [30] is of great importance for the analysis of deep actuators. Finally, we represent in Figure 6 the distribution of tangential and transverse midsurface displacements in the θ_2-direction.

7.2 Geometrically Non-Linear Examples

7.2.1 Cantilever Plate with Segmented Actuators

For the finite deformation analysis, we apply the total voltage $\hat{\varphi} = 1576\,\mathrm{V}$ in one load step. Figure 7 shows a voltage-displacement curve of the $[0/45/-45]_s$ plate compared with the finite element solution [6]. One can observe that again all results agree closely but the EG7P4 element is less expensive owing to the economical derivation of its stiffness matrix. Moreover, the EG7P4 element requires only one load step to find a converged solution of this highly non-linear problem. Table 3 lists additionally the results of the convergence study through using the Euclidean norms of the residual vector RN and displacement vector DN.

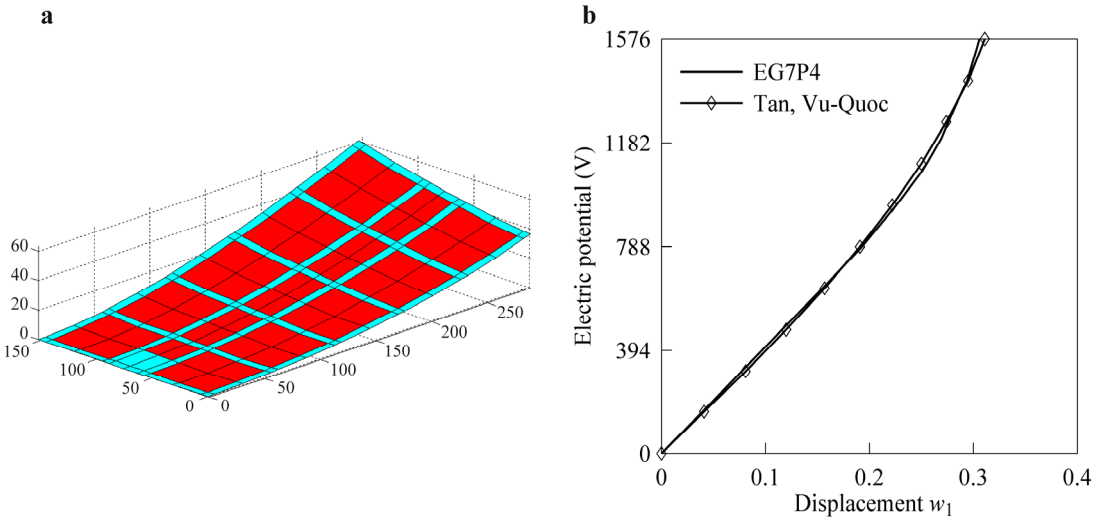

Figure 7: Cantilever $[0/45/-45]_s$ plate in bending actuation: (a) deformed configuration at applied voltage $\hat{\varphi} = 1576\,\mathrm{V}$ and (b) non-linear voltage-displacement curve

NI	0	1	2	3	4	5	6	7	8	9	10
RN	3.9E+6	2.1E+7	1.5E+6	9.2E+6	1.5E+7	1.0E+6	4.5E+5	6.1E+4	2.3E+3	2.7E-3	3.0E-4
DN	8.9E-1	1.8E-1	5.5E-1	7.5E-1	1.2E-1	5.6E-2	1.6E-2	7.1E-4	6.3E-6	1.4E-10	9.5E-11

Table 3: Convergence results for the cantilever $[0/45/-45]_s$ plate when the total voltage $\hat{\varphi} = 1576\,\mathrm{V}$ is applied in one load step

7.2.2 Shape Control of Pinched Hyperbolic Shell with Piezoelectric Patches Undergoing Finite Rotations

Consider a three-layer cross-ply hyperbolic shell under two pairs of opposite forces (Figure 8). This problem was studied by Basar et al. [31] for testing the finite rotation shell formulations, while we employ a hyperbolic shell example to assess the possibility of controlling the shape of laminated shells with segmented piezoelectric patches subjected to arbitrarily large actuation. Such an example is also an excellent test to verify the proper representation of inextensional bending and the ability of the element to model large rigid-body motions. Note that the results of solving this demanding benchmark through the purely mechanical EG7P4 element are documented in [19].

The shell core is composed of three composite layers with ply thicknesses of $[h_1/h_2/h_3]$, where $h_n = h_C/3$, and ply orientations of [90/0/90], that is, fiber directions coincide with the θ_2-direction in outer layers. The shape control of the three-layer hyperbolic shell is achieved with the help of eight piezoelectric patches of the thickness $h_{PZT} = 0.01\mathrm{cm}$ attached at inner and outer surfaces and located at the force point as depicted in Figure 8. The geometrical data of the shell are taken to be typical in the finite element literature: $r = 7.5\,\mathrm{cm}$, $R = 15\,\mathrm{cm}$, $L = 20\,\mathrm{cm}$ and $h_C = 0.04\,\mathrm{cm}$. The material properties of the composite [31] and piezoceramic (future developments) are listed in Table 1. The piezoceramic patches are polarized in opposite directions parallel to the θ_3-direction and subjected to a constant voltage $\hat{\varphi}$ to induce the bending actuation. As usual the electrodes on interfaces are grounded.

Due to symmetry of the problem, only one octant of the shell is discretized with the 16×16 mesh of EG7P4 elements. Figure 9 displays undeformed and deformed configurations of the shell under mechanical loading $F = 200\,\mathrm{N}$ and electrical loading $\hat{\varphi} = 1000\,\mathrm{V}$ and $1960\,\mathrm{V}$ as well. It is seen that the electric potential of $1960\,\mathrm{V}$ applied to outer patches surfaces returns the shell to its initial configuration. To investigate a problem of the shape control more carefully, we represent in Figure 10 the midsurface displacements at points A, B, C and D, where u_x and u_y denote displacements in *x*- and *y*-directions. Figure 11 shows additionally the distribution of midsurface displacements along hyperbolas BD and AC for different values of the electric potential. The data listed in Table 4 exhibit again the monotonic and quick convergence of the Newton-Raphson method for a very high level of loading.

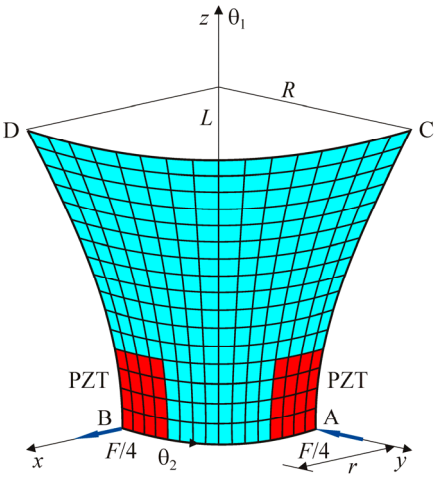

Figure 8: One octant of the three-layer hyperbolic shell with segmented actuators: geometry and mesh configuration

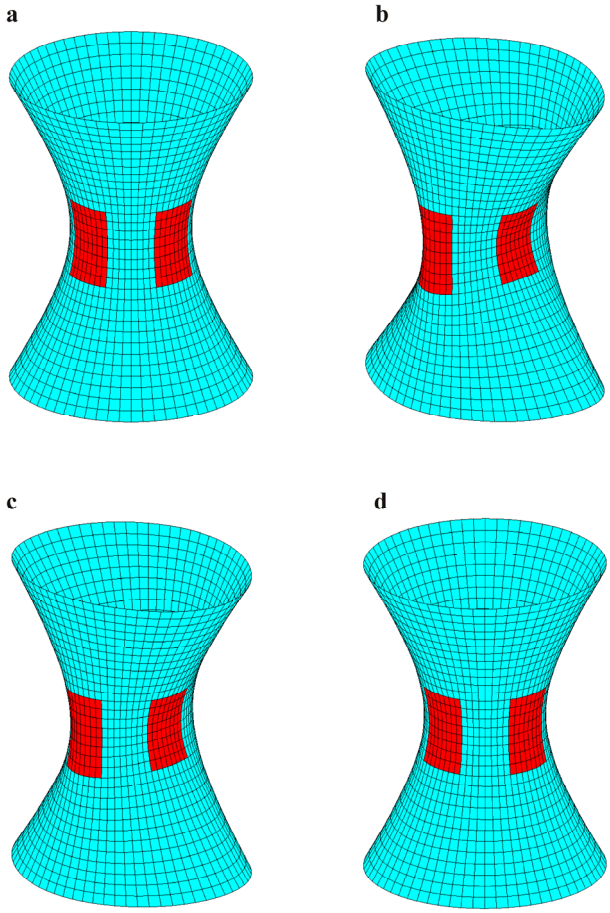

Figure 9: Three-layer hyperbolic shell at applied loads: (a) $F = 0$ and $\hat{\varphi} = 0$, (b) $F = 200\,\mathrm{N}$ and $\hat{\varphi} = 0$, (c) $F = 200\,\mathrm{N}$ and $\hat{\varphi} = 1000\,\mathrm{V}$, and (d) $F = 200\,\mathrm{N}$ and $\hat{\varphi} = 1960\,\mathrm{V}$

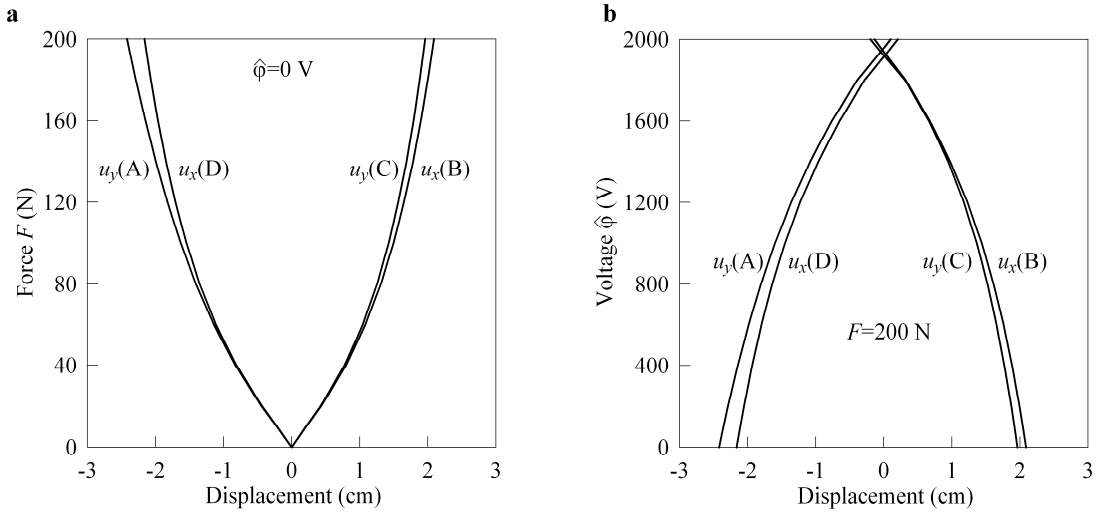

Figure 10: Three-layer hyperbolic shell. Midsurface displacements at points A, B, C and D versus: (a) force F for $\hat{\varphi} = 0$ and (b) voltage $\hat{\varphi}$ for $F = 200\,\mathrm{N}$

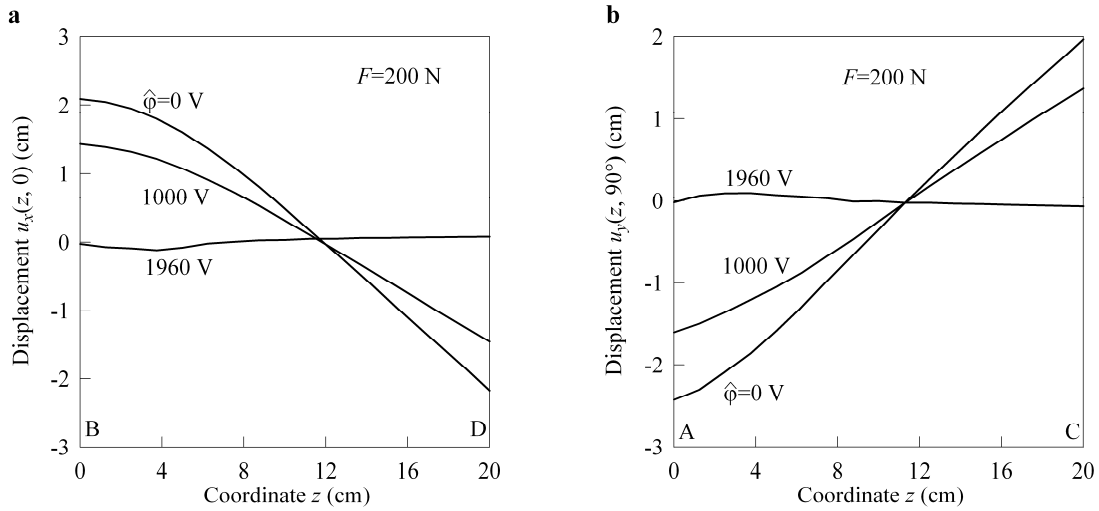

Figure 11: Three-layer hyperbolic shell. Midsurface displacements at points belonging to: (a) hyperbola BD and (b) hyperbola AC

NI	0	1	2	3	4	5	6	7	8	9
RN	1.3E+6	1.1E+5	1.4E+4	1.2E+5	5.3E+4	7.5E+3	2.2E+2	4.7E-1	5.7E-6	8.8E-8
DN	7.3E-3	1.3E-2	9.8E-2	6.9E-2	2.3E-2	4.1E-3	1.4E-4	5.9E-7	9.4E-10	9.3E-10

Table 4: Convergence results for the three-layer hyperbolic shell when the total load $P = 200$ N and the total voltage $\hat{\varphi} = 1960$ V are applied in one load step

8 Conclusions

A new finite rotation piezoelectric laminated solid-shell model has been developed. This model is based on the objective strain-displacement relationships of the first-order 7-parameter ESL shell theory, which are invariant under arbitrarily large rigid-

body shell motions. The simple and efficient EG hybrid stress-strain piezoelectric curved four-node solid-shell element is based on the original approach in which displacement vectors of outer and middle surfaces are introduced but resolved, in contrast with the isoparametric solid-shell element formulation, in the reference surface frame. It is remarkable that all elemental matrices require only direct substitutions and they are evaluated by using the 3D analytical integration. So, our EG piezoelectric solid-shell element is economical compared to conventional isoparametric hybrid/mixed piezoelectric finite elements because it additionally permits using coarse mesh configurations. Taking into account that electric signals generated by sensors are fed into microprocessors to activate a system of piezoelectric actuators in real time, a developed code is robust and promising.

Acknowledgment

The support of this work by Russian Ministry of Education and Science under Grant No 2.1.1/660 is gratefully acknowledged.

References

[1] K.Y. Sze, L.Q. Yao, "Modelling Smart Structures with Segmented Piezoelectric Sensors and Actuators", Journal of Sound and Vibration, 235, 495-520, 2000.

[2] K.Y. Sze, L.Q. Yao, S. Yi, "A Hybrid Stress ANS Solid-Shell Element and its Generalization for Smart Structure Modelling. Part II – Smart Structure Modelling", International Journal for Numerical Methods in Engineering, 48, 565-582, 2000.

[3] S. Lee, C. Cho, H.C. Park, K.J. Yoon, N.S. Goo, "Analysis of Multi-Layered Actuators Using an Assumed Strain Solid Element". Materials Chemistry and Physics, 75, 174-177, 2002.

[4] S. Lee, N.S. Goo, H.C. Park, K.J. Yoon, C. Cho, "A Nine-Node Assumed Strain Shell Element for Analysis of a Coupled Electro-Mechanical System", Smart Materials and Structures, 12, 355-362, 2003.

[5] S. Zheng, X. Wang, W. Chen, "The Formulation of a Refined Hybrid Enhanced Assumed Strain Solid Shell Element and its Application to Model Smart Structures Containing Distributed Piezoelectric Sensors/Actuators", Smart Materials and Structures, 13, N43-N50, 2004.

[6] X.G. Tan, L. Vu-Quoc, "Optimal Solid Shell Element for Large Deformable Composite Structures with Piezoelectric Layers and Active Vibration Control", International Journal for Numerical Methods in Engineering, 64, 1981-2013, 2005.

[7] S. Klinkel, W. Wagner, "A Geometrically Non-Linear Piezoelectric Solid Shell Element Based on a Mixed Multi-Field Variational Formulation", International Journal for Numerical Methods in Engineering, 65, 349-382, 2006.

[8] S. Klinkel, W. Wagner, "A Piezoelectric Solid Shell Element Based on a Mixed Variational Formulation for Geometrically Linear and Nonlinear Ap-

plications", Computers & Structures, 86, 38-46, 2008.
[9] S. Lentzen, "Nonlinearly Coupled Thermopiezoelectric Modelling and FE-Simulation of Smart Structures", Fortschritt-Berichte VDI, Reihe 20, Nr. 419, VDI Verlag, Düsseldorf, 2009.
[10] T.H.H. Pian, "Finite Elements Based on Consistently Assumed Stresses and Displacements", Finite Elements in Analysis and Design, 1, 131-140, 1985.
[11] N. Buchter, E. Ramm, D. Roehl, "Three-Dimensional Extension of Nonlinear Shell Formulation Based on the Enhanced Assumed Strain Concept", International Journal for Numerical Methods in Engineering, 37, 2551-2568, 1994.
[12] G.M. Kulikov, S.V. Plotnikova, "Geometrically Exact Four-Node Piezoelectric Solid-Shell Element", Mechanics of Advanced Materials and Structures, 15, 199-207, 2008.
[13] G.M. Kulikov, S.V. Plotnikova, "Exact Geometry Piezoelectric Solid-Shell Element Based on the 7-Parameter Model", Mechanics of Advanced Materials and Structures, 17, 2010 (in print).
[14] H. Parisch, "A Continuum-Based Shell Theory for Non-Linear Applications", International Journal for Numerical Methods in Engineering, 38, 1855-1883, 1995.
[15] N. El-Abbasi, S.A. Meguid, "A New Shell Element Accounting for Through-Thickness Deformation", Computer Methods in Applied Mechanics and Engineering, 189, 841-862, 2000.
[16] B. Brank, "Nonlinear Shell Models with Seven Kinematic Parameters", Computer Methods in Applied Mechanics and Engineering, 194, 2336-2362, 2005.
[17] R.A. Arciniega, J.N. Reddy, "Tensor-Based Finite Element Formulation for Geometrically Nonlinear Analysis of Shell Structures", Computer Methods in Applied Mechanics and Engineering, 196, 1048-1073, 2007.
[18] G.M. Kulikov, S.V. Plotnikova, "Equivalent Single-Layer and Layer-Wise Shell Theories and Rigid-Body Motions – Part I: Foundations", Mechanics of Advanced Materials and Structures, 12, 275-283, 2005.
[19] G.M. Kulikov, S.V. Plotnikova, "Finite Rotation Geometrically Exact Four-Node Solid-Shell Element with Seven Displacement Degrees of Freedom", Computer Modeling in Engineering & Sciences, 28, 15-38, 2008.
[20] G.M. Kulikov, "Strain-Displacement Relationships that Exactly Represent Large Rigid Displacements of a Shell", Solid Mechanics, 39, 105-113, 2004.
[21] G.M. Kulikov, E. Carrera, "Finite Deformation Higher-Order Shell Models and Rigid-Body Motions", International Journal of Solids and Structures, 45, 3153-3172, 2008.
[22] K.Y. Sze, X.-M. Yang, H. Fan, "Electric Assumption for Piezoelectric Laminate Analysis", International Journal of Solids and Structures, 41, 2363-2382, 2004.
[23] S.V. Gopinathan, V.V. Varadan, V.K. Varadan, "A Review and Critique of Theories for Piezoelectric Laminates", Smart Materials and Structures, 9, 24-48, 2000.
[24] A. Benjeddou, J.-F. Deü, S. Letombe, "Free Vibrations of Simply-Supported Piezoelectric Adaptive Plates: an Exact Sandwich Formulation", Thin-Walled Structures, 40, 573-593, 2002.

[25] G.M. Kulikov, S.V. Plotnikova, “Non-Linear Strain-Displacement Equations Exactly Representing Large Rigid-Body Motions. Part I. Timoshenko-Mindlin Shell Theory”, Computer Methods in Applied Mechanics and Engineering, 192, 851-875, 2003.
[26] G.M. Kulikov, S.V. Plotnikova, “Non-Linear Strain-Displacement Equations Exactly Representing Large Rigid-Body Motions. Part II. Enhanced Finite Element Technique”, Computer Methods in Applied Mechanics and Engineering, 195, 2209-2230, 2006.
[27] G.M. Kulikov, S.V. Plotnikova, “Non-Linear Geometrically Exact Assumed Stress-Strain Four-Node Solid-Shell Element with High Coarse-Mesh Accuracy”, Finite Elements in Analysis and Design, 43, 425-443, 2007.
[28] H.S. Tzou, “Piezoelectric Shells: Distributed Sensing and Control of Continua”, Kluwer-Academic, Dordrecht, 1993.
[29] E.F. Crawley, K.B. Lazarus, “Induced Strain Actuation of Isotropic and Anisotropic Plates”, AIAA Journal, 29, 944–951, 1991.
[30] W. Zouari, T. Ben Zineb, A. Benjeddou, “A FSDT-MITC Piezoelectric Shell Finite Element with Ferroelectric Non-Linearity”, Journal of Intelligent Material Systems and Structures, 20, 2055-2075, 2009.
[31] Y. Basar, Y. Ding, R. Schultz, “Refined Shear-Deformation Models for Composite Laminates with Finite Rotations”, International Journal of Solids and Structures, 30, 2611-2638, 1993.

Appendix A

The mechanical, piezoelectric and dielectric constitutive matrices introduced in Section 5 are given by

$$\mathbf{D}_{uu} = \begin{bmatrix} D_{11}^{00} & D_{11}^{01} & D_{12}^{00} & D_{12}^{01} & D_{13}^{00} & D_{13}^{01} & D_{16}^{00} & D_{16}^{01} & 0 & 0 \\ & D_{11}^{11} & D_{12}^{01} & D_{12}^{11} & D_{13}^{01} & D_{13}^{11} & D_{16}^{01} & D_{16}^{11} & 0 & 0 \\ & & D_{22}^{00} & D_{22}^{01} & D_{23}^{00} & D_{23}^{01} & D_{26}^{00} & D_{26}^{01} & 0 & 0 \\ & & & D_{22}^{11} & D_{23}^{01} & D_{23}^{11} & D_{26}^{01} & D_{26}^{11} & 0 & 0 \\ & & & & D_{33}^{00} & D_{33}^{01} & D_{36}^{00} & D_{36}^{01} & 0 & 0 \\ & & & & & D_{33}^{11} & D_{36}^{01} & D_{36}^{11} & 0 & 0 \\ & & & & & & D_{66}^{00} & D_{66}^{01} & 0 & 0 \\ & & & & & & & D_{66}^{11} & 0 & 0 \\ & & & & & & & & D_{55} & D_{45} \\ \text{sym.} & & & & & & & & & D_{44} \end{bmatrix},$$

$$\mathbf{D}_{u\varphi}^{(\ell)}=\begin{bmatrix} 0 & 0 & 0 & 0 & m_\ell^0 e_{31}^{(\ell)} \\ 0 & 0 & 0 & 0 & m_\ell^1 e_{31}^{(\ell)} \\ 0 & 0 & 0 & 0 & m_\ell^0 e_{32}^{(\ell)} \\ 0 & 0 & 0 & 0 & m_\ell^1 e_{32}^{(\ell)} \\ 0 & 0 & 0 & 0 & m_\ell^0 e_{33}^{(\ell)} \\ 0 & 0 & 0 & 0 & m_\ell^1 e_{33}^{(\ell)} \\ 0 & 0 & 0 & 0 & m_\ell^0 e_{36}^{(\ell)} \\ 0 & 0 & 0 & 0 & m_\ell^1 e_{36}^{(\ell)} \\ k_\ell^0 e_{15}^{(\ell)} & k_\ell^1 e_{15}^{(\ell)} & k_\ell^0 e_{25}^{(\ell)} & k_\ell^1 e_{25}^{(\ell)} & 0 \\ k_\ell^0 e_{14}^{(\ell)} & k_\ell^1 e_{14}^{(\ell)} & k_\ell^0 e_{24}^{(\ell)} & k_\ell^1 e_{24}^{(\ell)} & 0 \end{bmatrix},$$

$$\mathbf{D}_{\varphi\varphi}^{(\ell)}=\begin{bmatrix} k_\ell^{00}\in_{11}^{(\ell)} & k_\ell^{01}\in_{11}^{(\ell)} & k_\ell^{00}\in_{12}^{(\ell)} & k_\ell^{01}\in_{12}^{(\ell)} & 0 \\ & k_\ell^{11}\in_{11}^{(\ell)} & k_\ell^{01}\in_{12}^{(\ell)} & k_\ell^{11}\in_{12}^{(\ell)} & 0 \\ & & k_\ell^{00}\in_{22}^{(\ell)} & k_\ell^{01}\in_{22}^{(\ell)} & 0 \\ & & & k_\ell^{11}\in_{22}^{(\ell)} & 0 \\ \text{sym.} & & & & h_\ell\in_{33}^{(\ell)} \end{bmatrix},$$

$$D_{ab}^{pq}=\sum_n m_n^{pq}C_{ab}^{(n)},\qquad D_{cd}=\sum_n h_n C_{cd}^{(n)},$$

$$m_n^{pq}=\int_{z_{n-1}}^{z_n}\left(N^-\right)^{2-p-q}\left(N^+\right)^{p+q}d\theta_3,\qquad m_\ell^p=\int_{z_{\ell-1}}^{z_\ell}\left(N^-\right)^{1-p}\left(N^+\right)^{p}d\theta_3,$$

$$k_\ell^{pq}=\int_{z_{\ell-1}}^{z_\ell}\left(N_\ell^-\right)^{2-p-q}\left(N_\ell^+\right)^{p+q}d\theta_3,\qquad k_\ell^{p}=\int_{z_{\ell-1}}^{z_\ell}\left(N_\ell^-\right)^{1-p}\left(N_\ell^+\right)^{p}d\theta_3=\frac{1}{2}h_\ell,$$

where $a,b=1,2,3,6$ and $c,d=4,5$, and $p,q=0,1$.